https://dx.doi.org/10.1016/j.scitotenv.2021.149603

Photochemical ozone pollution in five Chinese megacities in summer 2018

Xufei Liu[1], Hai Guo[1*], Lewei, Zeng[1], Xiaopu Lyu[1], Yu Wang[2], Yangzong Zeren[1], Jin Yang[1], Luyao Zhang[1], Shizhen Zhao[3], Jun Li[3], Gan Zhang[3]

[1] Air Quality Studies, Department of Civil and Environmental Engineering, Hong Kong Polytechnic University, Hong Kong, China

[2] Institute for Environmental and Climate Research, Jinan University, Guangzhou, China

[3] Guangzhou Institute of Geochemistry, Chinese Academy of Sciences, Guangzhou, China

* Corresponding author. ceguohai@polyu.edu.hk

Abstract

To investigate photochemical ozone (O_3) pollution in urban areas in China, O_3 and its precursors and meteorological parameters were simultaneously measured in five megacities in China in summer 2018. Moderate wind speeds, strong solar radiation and high temperature were observed in all cities, indicating favorable meteorological conditions for local O_3 formation. However, the unusually frequent precipitation caused by typhoons reaching the eastern coastline resulted in the least severe air pollution in Shanghai. The highest O_3 level was found in Beijing, followed by Lanzhou and Wuhan, while relatively lower O_3 value was recorded in Chengdu and Shanghai. Photochemical box model simulations revealed that net O_3 production rate in Lanzhou was the largest, followed by Beijing, Wuhan and Chengdu, while it was the lowest in Shanghai. Besides, the O_3 formation was mainly controlled by volatile organic compounds (VOCs) in most cities, but co-limited by VOCs and nitrogen oxides in Lanzhou. Moreover, the dominant VOC groups contributing to O_3 formation were oxygenated VOCs (OVOCs) in Beijing and Wuhan, alkenes in Lanzhou, and aromatics and OVOCs in Shanghai and Chengdu. Source apportionment analysis identified six sources of O_3 precursors in these cities, including liquefied petroleum gas usage, diesel exhaust, gasoline exhaust, industrial emissions, solvent usage, and biogenic emissions. Gasoline exhaust dominated the O_3 formation in Beijing, and LPG usage and industrial emissions made comparable contributions in Lanzhou, while LPG usage and solvent usage played a leading role in Wuhan and Chengdu, respectively. The findings are helpful to mitigate O_3 pollution in China.

Keyword: Ozone formation, VOCs, radical chemistry, PBM-MCM, megacity clusters.

1. Introduction

Ozone (O_3) pollution has attracted increasing attention in China since it has adverse impact on human health (Bell et al., 2004), agriculture (Ashmore, et al., 2005; Wang et al., 2005) and air quality (Thompson et al., 2011). Tropospheric O_3 is produced through complex chemical reactions between its precursors, *i.e.*, volatile organic compounds (VOCs) and nitrogen oxides (NO_x), under the sunlight. However, the nonlinear relationship between O_3 and its precursors makes it difficult to control O_3 formation (NRC, 1992; Carter, 1994).

Severe O_3 pollution has been frequently observed in warm seasons in many megacities of China (Wang T. et al., 2017; Wu and Xie, 2017; Li K et al., 2019). Over the past 20 years, a large number of studies have reported the increasing O_3 trends and strong photochemical reactions in several highly urbanized regions (Wang T. et al., 2017; Wang W. et al., 2017; Lu et al., 2020a), such as North China Plain (NCP) (Zhang et al., 2014; Tan et al., 2017, 2018a; Yang et al., 2018), Yangtze River Delta (YRD) (Tang et al., 2008; Ran et al., 2009, 2012; Zhu J. et al., 2020), and Pearl River Delta (PRD) (Wang Y et al., 2017; Lu X. et al., 2019; Liu and Wang, 2020a, b; Yang et al., 2020). Moreover, cities in central and western China also experience air quality deterioration, especially photochemical pollution, due to their expansion of economy, population, and industrialization, such as Wuhan (Lyu et al., 2016a; Hui et al., 2018; Zeng et al., 2018), Chengdu (Su et al., 2017; Tan et al., 2018b; Ning et al., 2020) and Lanzhou (Xue et al., 2014a; Jia et al., 2016). Since 2013, the central government has made great effort to fight against the air pollution problem in China, including various stringent control strategies on multiple anthropogenic pollutants, *e.g.,* the Air Pollution Prevention and Control Action Plan in 2013-2018 (MEE PRC, 2019), the short-run "Blue Sky Defense Battle" from 2018 to 2020 (MEE PRC, 2018) and the long-run "Beautiful China Scheme" until 2035 (CCIED, 2019) According to Lu et al. (2020b), though many pollutants such as SO_2 and $PM_{2.5}$ have been effectively controlled, O_3 pollution is still increasing in urban areas in China, indicating that

corresponding control measures on O_3 precursors, *i.e.*, VOCs and NO_x, in different cities should be more targeted and rigorous.

Moreover, since each city has its unique industrial structures, energy use pattern and meteorological conditions, the photochemical O_3 formation mechanisms in different cities may be different, which must be considered when formulating O_3 control strategies (Lu H. et al., 2019; Wang et al., 2019). In the past decade, many studies have investigated the net O_3 production rate and/or radical chemistry in the urban areas of Chinese megacities. For instance, an average daytime net O_3 production rate of 25.8 ppbv h^{-1} was reported by Liu et al. (2012) at an urban site in Beijing in summer 2007, and photolysis of VOCs dominated the local formation of OH radical. Based on measurement data at an urban site in Wuhan in autumn 2013, Lu et al. (2017) found that the daytime mean net O_3 production rate was 8.8 ppbv h^{-1} and highlighted the significant contribution of nitrous acid (HONO) to the atmospheric oxidative capacity in central China. Most recently, Zeng et al. (2019) applied an observation-based model to explore the O_3 photochemistry at an urban site in Wuhan in summer 2016 and indicated the average daily peak net O_3 production rate of 10 ppbv h^{-1}. However, the radical chemistry was not investigated in this study. Tan et al.(2018b) first revealed the peak net O_3 production rate of 20 - 28 ppbv h^{-1} at four urban/suburban sites of Chengdu in autumn 2016. Moreover, they analyzed the RO_x budget using simulated radical concentrations and proved severe O_3 pollution based on comprehensive radical chemistry in southwestern China. However, there is a dearth of nationwide studies on in-situ O_3 photochemistry in urban areas of major Chinese megacities, especially in central and western China, not to mention simultaneous study in multiple cities in China.

In the past decades, China has experienced rapid industrialization and urbanization, which accelerated the consumption of energy, enlarged the emissions of VOCs, and led to more O_3 production (Li M. et al., 2019; Tan et al., 2018b; Xu et al., 2019). A variety of natural and anthropogenic sources, which directly emit hundreds of VOC species into the atmosphere and contribute differently to local O_3 formation, have been extensively studied to examine their impact on air quality in China (Jia et al., 2016; Lyu et al., 2016b; Guo et al., 2017; Wang T. et

al., 2017; Song et al., 2018; Liu Y. et al., 2019). For example, Wang et al. (2010) identified six VOC sources in summer Beijing, including vehicle exhaust, liquefied petroleum gas (LPG) usage, gasoline evaporation, biogenic emission, paint and solvents, and chemical industry, among which vehicle exhaust contributed the most to VOCs (57-60%), followed by LPG usage (10-19%) and gasoline evaporation (7-17%). The largest contribution of vehicular emissions was also found in Wuhan (27.8%; Lyu et al., 2016b) and Chengdu (45.0%; Song et al., 2018). Five out of six sources identified in Wuhan and Chengdu, respectively, were the same as those in Beijing (Wang et al., 2010), except for gasoline evaporation replaced by coal burning in Wuhan (Lyu et al., 2016b) and LPG usage replaced by a second industrial source in Chengdu (Song et al., 2018). As reported by Liu Y. et al. (2019), petrochemical industry was the largest contributor to VOCs in Shanghai (35.6%). Given that Lanzhou is a highly industrialized city, Jia et al. (2016) reported that the mixed industrial processes in Lanzhou contributed the most to VOCs (26.8%). The different VOC sources among cities may be partially affected by the different sampling seasons and industrial structures of the cities. However, there is a lack of studies that simultaneously investigate the spatial variations of VOC sources and their contributions to O_3 formation in urban areas of multiple megacities in China, particularly in warm seasons.

In this study, intensive measurements of O_3 and its precursors were simultaneously conducted in urban areas in five megacities, including Beijing, Shanghai, Wuhan, Chengdu, and Lanzhou, in summer 2018. Through comprehensive data analysis, the chemical characteristics of O_3 and its precursors were investigated; the sensitivity of O_3 production to precursors and the production and destruction pathways of O_3 and radicals were evaluated with the aid of an observation-based photochemical box model; and the spatial variations of VOC sources and their contributions to local O_3 formation were quantified in each megacity. These findings are expected to help alleviate O_3 pollution across the country.

2. Methodology

2.1 Sampling sites

In this study, field measurements were undertaken in urban areas in five major city clusters of China in summer 2018, including North China Plain (NCP), Yangtze River Delta (YRD), central China, Sichuan Basin (SCB) and northwestern China (*i.e.,* Beijing, Shanghai, Wuhan, Chengdu and Lanzhou, respectively) (Figure 1). The sampling site in each megacity was chosen based on the following criteria. Firstly, a residential or commercial area was determined to represent the urban environment in each city. Secondly, the sampling site was in an open and high location without tall buildings and/or trees blocking the movement of air mass. Thirdly, there were no emission sources (e.g., chimneys, vents, etc.) around the sampling site. Lastly, the locations close to national air monitoring stations were preferable. Table S1 gives the detailed information and descriptions of the environments around the five urban sites in the megacities. Note we defined O_3 episode days as the day when maximum hourly mixing ratio of O_3 exceeded 100 ppbv (Level II of National Ambient Air Quality Standard in China).

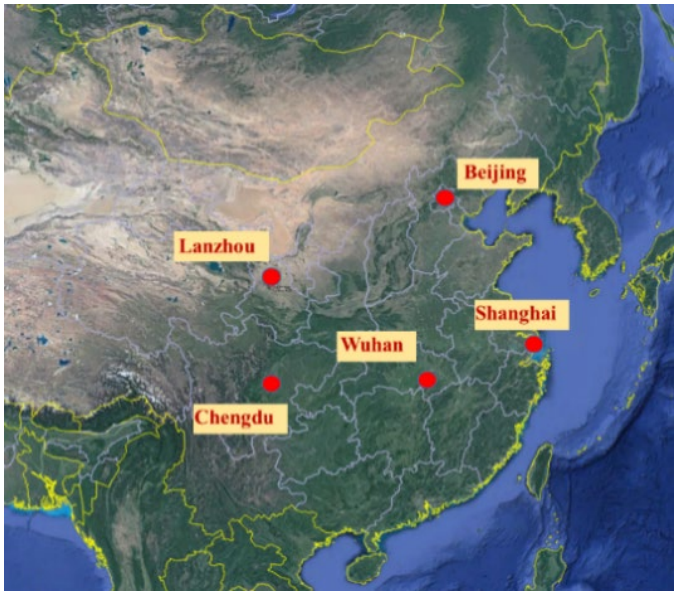

Figure 1. Maps showing the locations of the five megacities in China, *i.e.*, Beijing, Shanghai, Wuhan, Chengdu, and Lanzhou.

2.2 Sampling and VOC analysis

Continuous measurements of trace gases (*i.e.,* O_3, CO and NO-NO_2-NO_x) and meteorological parameters (*i.e.,* solar radiation, relative humidity, temperature, wind speed and wind direction) were conducted at each site in August 2018. Different instruments for trace gases measurements at each sampling site were applied during this comprehensive sampling

campaign (Table S2). The high-resolution observation data were averaged into hourly values. In addition, the meteorological variables were synchronously monitored by weather stations of model QS/T 1-2000 at Beijing and Shanghai sites and mini weather stations (model HX-2000) in Wuhan, Chengdu and Lanzhou, respectively.

On selected sampling days, hourly whole-air samples were collected using pre-cleaned and vacuumed 2L canisters every other hour from 08:00 to 19:00 LT at each site, *i.e.,* six hourly VOC samples were obtained every day. In total, 207 VOCs and 209 OVOC samples were obtained in the five cities (Table S1). These VOC samples were analyzed using gas chromatography coupled with mass spectrometry, electron capture detection and flame ionization detection (GC-MSD-ECD-FID) in Hong Kong Polytechnic University. In addition, we collected oxygenated VOCs (OVOC) using dinitrophenylhydrazine (DNPH)-silica cartridges (Waters, Milford, MA) for 2 hours at a flow rate of 0.5 L min^{-1} every two hours during the daytime hours (08:00 – 18:00 LT). To avoid the influence of O_3 in the air on the sampled OVOCs, we connected an O_3 scrubber at the inlet of the DNPH cartridge and replaced it after collecting two samples. During the sampling period, the VOC canisters and DNPH-cartridges were shipped via speed logistics immediately after the sample collection. It took 2-4 weeks to deliver the samples from different sampling sites to the laboratory in Hong Kong. In this study, the mixing ratios of 44 speciated VOCs and 4 OVOCs (Table S3) were used for numerical simulations with a box model (see Section 2.3.2).

2.3 Description and configurations of models

2.3.1 Source apportionment

To identify VOC sources and quantify their contributions to ambient VOCs, a receptor model, *i.e.,* Positive Matrix Factorization (PMF), is often used (Lee et al., 1999; Brown et al., 2007). In this study, we used the USEPA PMF 5.0 model (USEPA, 2017) for source apportionment. Equation 1 below illustrates the basic principle of this model (Paatero, 1997; Ling et al., 2014).

$$x_{ij} = \sum_{k=1}^{p} g_{ik} f_{kj} + e_{ij} \quad \text{(Equation 1)}$$

where x_{ij} represents the observed value of jth species in ith sample, g_{ik} denotes the fraction of kth source in ith sample, f_{kj} is the percentage of jth species in kth source, and e_{ij} stands for the residual of jth species in ith sample. p is the total number of sources (Paatero, 2000a, b).

The PMF provides solutions with minimum Q values (Equation 2), which converge based on the uncertainties (u) of input data.

$$Q = \sum_{i=1}^{n} \sum_{j=1}^{m} \left[\frac{x_{ij} - \sum_{k=1}^{p} g_{ik} f_{kj}}{u_{ij}} \right]^2 \quad \text{(Equation 2)}$$

where u_{ij} denotes the uncertainty value of jth species in ith sample; n is the total number of samples, and m means the total number of species.

According to Polissar et al. (1998) and Reff et al. (2007), the uncertainties of the VOC mixing ratios applied to PMF in this study were set as follows. For VOC values lower than or equal to the limit of detection (LoD), half of the LoDs was used for corresponding species, while 5/6 of the corresponding LoDs were taken as the uncertainties of these VOC values. If the VOC values were higher than LoDs, Equation 3 was applied to calculate the uncertainties, in which the error fraction of 10% was assumed. Due to analytical and computational problems, mass spectrometry based datasets frequently contain missing values. This occurred for one or two species in very few canister samples in this study. To resolve this issue, the geometric mean of observed concentrations of a VOC was used to substitute any missing values of this VOC and the accompanying uncertainty was four times the geometric mean value. More information about the settings of the uncertainty can be found in Norris et al. (2008) and Zhang et al. (2012).

$$\text{Uncertainty} = [(\text{Error Fraction} \times \text{concentration})^2 + (\text{LoD})^2]^{1/2} \quad \text{(Equation 3)}$$

To obtain optimal solution, different number of factors were selected for testing in the model. For each test, the model was run at least 20 times and the seed was randomly chosen. Several criteria were considered before finally determining the best solution of the model: (1) a good agreement to the measurement data; and (2) the most interpretable source profile based on the information on the VOC sources in the sampling areas (Wang et al., 2010; Jia et al., 2016; Lyu et al., 2016b; Song et al., 2018; Liu X. et al., 2019; Liu Y. et al., 2019).

2.3.2 Photochemical box model

2.3.2.1 General description

To simulate how VOCs and OVOCs contribute to photochemical O_3 formation, a photochemical box model coupled with the near-explicit Master Chemical Mechanism (PBM-MCM) was applied in this study. The MCM v3.2 includes about 6,700 species and 17,000 reactions, and comprehensively describes the homogeneous gas-phase reactions in the atmosphere (Jenkin et al., 1997, 2003; Saunders et al., 2003). In this study, the hourly measurement data were input into the model, including temperature, relative humidity, trace gases and 48 C_2-C_{10} VOCs/OVOCs. The model was also localized to be suitable for each megacity. For example, the coordinates of each sampling site were taken into consideration when calculating the photolysis rates using Tropospheric Ultraviolet and Visible radiation (TUV) model based on the measured solar radiations (Madronich and Flocke, 1999; Wang Y. et al., 2017). Specifically, the actual location of each site and the modeling time periods were applied to assign an initial solar radiation with the default cloud optical depth (COD), aerosol optical depth (AOD), surface albedo and other parameters. Then, a calculated daily total solar radiation, which had a less than 1% difference from the observed value, could be obtained by adjusting different CODs progressively. Finally, the input configurations with the adjusted CODs were documented, and the corresponding photolysis rates O_3 (*i.e.,* $J(O^1D)$) and NO_2 (*i.e.,* $J(NO_2)$) were applied into PBM-MCM for photochemistry modeling. The planetary boundary layer with varying height was applied in the model during the daytime, *i.e.,* 300 m in early morning and late afternoon and 1400 m at noon. However, physical processes, *e.g.,* horizonal and vertical transport, were not considered in the model, which could cause insufficient evaluation of the air mass movement. Even so, previous studies demonstrated that the PBM-MCM had good performance in probing the in-situ photochemistry (Lam et al., 2013; Lyu et al., 2017a; Wang Y. et al., 2017, 2018; Liu X. et al., 2019, 2020).

2.3.2.2 Model performance

To assess the performance of the PBM-MCM model, the index of agreement (IOA) with range of 0 to 1, was applied (Equation 4) (Huang et al., 2005; Wang et al., 2015; Lyu et al., 2015, 2016b). The larger IOA value is, the better the model performs (Huang et al., 2005).

$$\mathrm{IOA} = 1 - \frac{\sum_{i=1}^{n}(O_i - S_i)^2}{\sum_{i=1}^{n}(|O_i - \tilde{O}| + |S_i - \tilde{O}|)^2} \quad \text{(Equation 4)}$$

where S_i represents simulated values, O_i denotes observed values, $\tilde{O}$ is the average value of all observation data, and n stands for the number of samples.

2.3.2.3 Evaluation of O_3-precursor relationship

Relative incremental reactivity (RIR) evaluates how O_3 precursors affect the O_3 formation (Cardelino and Chameides, 1995). RIR values, calculated from the simulated outputs of the PBM-MCM, can reflect the relative change in net O_3 production rate caused by the variation of mixing ratios of precursors. The positive RIR values indicate that the O_3 production would be effectively lessened by reducing the concentrations of the precursors. In this study, the O_3-integrated RIRs were applied given the weighted contributions to O_3 production. Equation 5 and Equation 6 are shown as follows:

$$RIR(X) = \frac{\left[P^S_{O_3-NO}(X) - P^S_{O_3-NO}(X-\Delta X)\right]/P^S_{O_3-NO}(X)}{\frac{\Delta S(X)}{S(X)}} \quad \text{(Equation 5)}$$

$$Integrated\ \ RIR(X) = \frac{\sum_{i=1}^{n}\left(RIR(X)_i \times O_{3_i}\right)}{\sum_{i=1}^{n} O_{3_i}} \quad \text{(Equation 6)}$$

where $\frac{\Delta S(X)}{S(X)}$ represents the hypothetical change of concentration of precursor X (*i.e.,* VOC species, CO or NO_x), assigned as 10% in this study; $P^S_{O_3-NO}(X)$ denotes the net O_3 production rate with original mixing ratios in the base run, while $P^S_{O_3-NO}(X-\Delta X)$ is the net O_3 production rate in the constrained run with 10% cutdown of species X but other species are not changed. $RIR(X)_i$ and O_{3_i} are the RIRs and simulated O_3 level at the i^{th} hour during a day, respectively. The calculation of net O_3 production rate, *i.e.,* $P^S_{O_3-NO}$, is illustrated in Equations 7 - 9 in Section 2.3.2.4.

2.3.2.4 Production and destruction pathways of O_3 and radicals

The PBM-MCM model was applied to simulate the production and destruction pathways and rates of O_3. The total production rate of O_3 was the sum of the oxidation rates of NO by both HO_2 and RO_2 (Equation 7), and the total destruction rate of O_3 was obtained by adding up the O_3 photolysis rate, reaction rates of OH with NO_2, and O_3 with OH, HO_2 and VOCs (Equation 8). By subtracting the total destruction rate from the total production rate, we can get the net O_3 production rate at each sampling site (Equation 9).

$$G_{O_3-NO} = k_{HO_2+NO}[HO_2][NO] + \sum k_{RO_2+NO}[RO_2][NO] \quad \text{(Equation 7)}$$

$$D_{O_3-NO} = k_{HO_2+O_3}[HO_2]\,[O_3] + k_{OH+O_3}[OH]\,[O_3] + k_{O(^1D)+H_2O}[O(^1D)][O_3] + k_{OH+NO_2}[OH]\,[NO_2] + k_{alkenes+O_3}[alkenes]\,[O_3] \quad \text{(Equation 8)}$$

$$P_{O_3-NO} = G_{O_3-NO} - D_{O_3-NO} \quad \text{(Equation 9)}$$

where, P_{O_3-NO} is the net O_3 production rate, G_{O_3-NO} is O_3 production rate and D_{O_3-NO} represents O_3 destruction rate. $O(^1D)$, NO and NO_2 in instantaneous steady state are assumed. The *k* values denote the rate constants of each reaction. The concentration and the production and destruction rates of radicals can also be simulated using the PBM-MCM model.

2.3.3 Simulation scenarios

To quantify the contribution of each VOC source to the O_3 production in five megacities, two simulation scenarios of PBM-MCM model at each sampling site were conducted. Specifically, Scenario 1 represented the O_3 photochemistry with whole-air samples, where the model was constrained by all O_3 precursors (excluding O_3). In Scenario 2, with six sub-scenarios related to six identified VOC sources, the VOCs from each individual source were subtracted from the model input. In this approach, the difference of simulated O_3 between Scenario 1 and each sub-Scenario 2 was regarded as the contribution of individual VOC sources to the local O_3 production at each sampling site. Bearing in mind that this approach could only qualitatively but not quantitatively calculate the contributions of VOC sources to O_3 production since photochemical O_3 is non-linearly correlated to its precursors. More detailed explanation is provided in Liu X. et al. (2019).

3. Results and discussion

3.1 Observation overview

During the sampling period, 6 – 8 days were selected to collect VOC samples in each city, among which 0 – 5 O_3 episode days were captured. It is noteworthy that the representativeness of the VOC data collected on a few days was considered. Prior to the sampling campaign we reviewed available literature to obtain the general characteristics of O_3 pollution in these five cities and identified August as a typical month to investigate O_3 pollution. Indeed, the levels of air pollutants including VOCs during the short-term period in all cities were comparable to those reported in previous studies as discussed below, revealing that further analysis of O_3 formation mechanisms and radical chemistry in the cities was typical. Figure 2 presents the daytime (08:00-18:00LT) variations of O_3, CO, NO_x, VOC groups and meteorological parameters on the VOC sampling days in the five cities in August 2018. Table S4 summarizes the daytime average values of air pollutants and meteorological parameters in the five cities. Here the TVOCs and VOC groups refer to the 44 VOCs and 4 OVOCs listed in Table S3. During the sampling period, 5 and 4 O_3 episode days were captured in Beijing and Lanzhou, respectively, while only 0-2 O_3 episode days were found in the other cities (Figure 2). It was found that Beijing had the highest O_3 mixing ratios (78.6±7.3 ppbv) ($p < 0.05$), followed by Lanzhou (67.2±7.8 ppbv) and Wuhan (63.9±6.8 ppbv), indicating the severe O_3 pollution in northern and central China in summer. The lower O_3 in Chengdu (52.5±7.5 ppbv) than in Beijing and Lanzhou ($p < 0.05$) was partly attributed to the stronger NO titration effect (NO_x: 23.8±2.8 ppbv vs. 18.8±1.5 ppbv (Beijing) and 18.2±2.4 ppbv (Lanzhou); $p<0.05$) and lower TVOCs levels (32.7±3.7 ppbv vs. 44.2±4.3 ppbv (Beijing) and 45.3±5.9 (Lanzhou); $p<0.05$), while the higher O_3 in Wuhan than in Chengdu ($p < 0.05$) was likely caused by higher temperature ($p < 0.05$) as both NO_x and TVOCs levels were comparable ($p = 0.36$) in these two cities. During the sampling period, Shanghai had the lowest levels of air pollutants with O_3 mixing ratio of 20.7±1.9 ppbv, which was mainly due to the unstable weather conditions with continuous precipitation caused by a few tropical storms over the East China Sea (CMA, 2019). In addition, moderate wind speeds (<2.0 m s^{-1}), strong solar radiation (359.4 – 385.5 W m^{-3})

and high ambient temperature (27.5 – 34.7 °C) in all the five cities suggested favorable meteorological conditions for local O_3 production in summer 2018.

During the sampling period, the cities in northern China, *i.e.*, Beijing and Lanzhou, had the largest TVOC concentrations (44.2±4.3 ppbv and 45.3±5.9 ppbv, respectively), followed by Chengdu in southwestern China (32.7±3.7 ppbv) and Wuhan in central China (30.2±3.1 ppbv), and Shanghai (19.1±1.9 ppbv) in eastern China had the lowest TVOCs. Among the four VOC groups, alkanes accounted for the highest proportions of TVOCs in Chengdu and Lanzhou (44.6-45.6%), while OVOCs ranked the first in Beijing (55.0%). Alkanes and OVOCs had similar contributions in Shanghai (alkanes: 31.9%; OVOCs: 35.6%; p = 0.11) and Wuhan (alkanes: 36.1%; OVOCs: 35.8%; p = 0.48). Furthermore, alkenes made the second contribution in Beijing (21.7%) and Lanzhou (27.8%), implying different chemical compositions in different cities though all the cities had severe O_3 pollution problem. Moreover, aromatics had the lowest proportions in all the five cities with percentages of 8.2-11.8%, in line with the range of 7-35% reported by previous publications in China (*e.g.,* Liu et al., 2008; Geng et al., 2009; Jia et al., 2016; Zhu et al., 2016).

In comparison, the levels of NO and NO_2 in the five cities were in line with other studies conducted in urban areas in China in summer. The mixing ratios of the measured TVOCs at multiple sites were within the range reported by previous studies at urban sites (*e.g.,* Duan et al., 2008; Cai et al., 2010; Han et al., 2015; Zou et al., 2015; Yang et al., 2018).

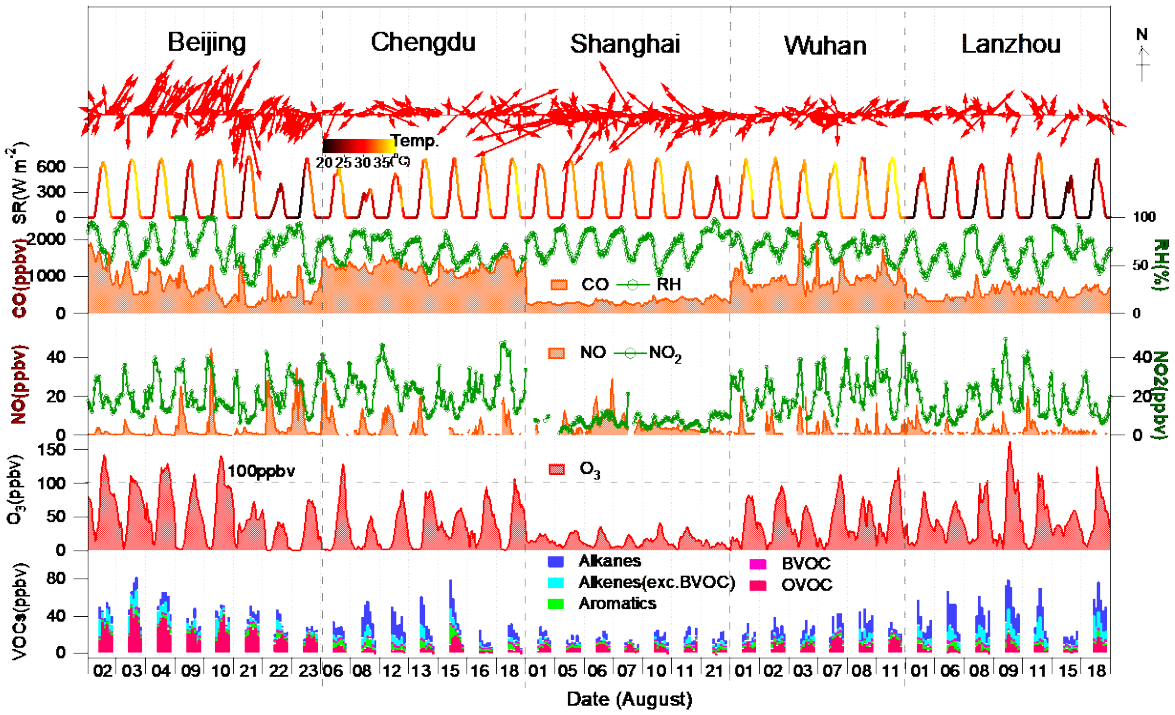

Figure 2. Temporal variations of trace gases (*i.e.,* O_3, CO, NO and NO_2), VOCs, and meteorological parameters in the five sampling cities, where SR, Temp. and RH refer to solar radiation, temperature and relative humidity, respectively.

3.2 O_3 photochemistry

3.2.1 Validation of model simulations

Prior to investigating the local O_3 photochemistry, the performance of PBM-MCM was evaluated. Figure S1 displays the daytime variations of observed O_3 and simulated mixing ratios on the VOC sampling days in summer 2018 in the five cities. The simulated O_3 agreed well with the observed O_3 variations with peaks at noon and lower values in the morning and evening. The IOA values in Beijing, Wuhan, Chengdu, and Lanzhou were between 0.74-0.88 (Table S5), within the ranges of 0.66-0.89 reported in previous studies (Lyu et al., 2015, 2016a, 2016b; Wang et al., 2015; Wang Y. et al., 2018; Liu X. et al., 2019). However, the IOA in Shanghai was a bit lower (0.61), probably because PBM-MCM usually performs better on high O_3 days with intense in-situ photochemical reactions (*e.g.,* Lam et al., 2013; Lyu et al., 2017a; Wang H. et al., 2018; Liu et al., 2020). The discrepancies between the observations and simulation results at all sites might be attributable to the physical processes, *e.g.,* horizontal

processes (including horizontal dispersion and horizontal advection) and vertical processes (including vertical dispersion, vertical advection and vertical mixing), which were not well covered in PBM-MCM (Wang Y. et al., 2017; Liu X. et al., 2019; Lyu et al., 2019). Note that PBM-MCM simulations were only constrained by O_3 precursors when simulating O_3 to evaluate the model performance (Section 3.2.1). However, PBM-MCM was constrained by the measurement data of both O_3 and its precursors when deciphering the photochemical oxidative reactions in this study, in which both regional transported and locally produced O_3 were taken into consideration by the model (Section 3.2.2 – Section 3.2.3).

3.2.2 In-situ net O_3 production

Figure 3 displays the average diurnal profiles of the simulated O_3 production and destruction rates in each city. The daytime average reaction rates and the contribution of each pathway are further illustrated in Table S6. Among the five cities, Lanzhou had the highest net O_3 production rate (8.9±1.7 ppbv h^{-1}) while Shanghai had the lowest value (2.8±0.7 ppbv h^{-1}) ($p < 0.05$). The net O_3 production rate in Beijing (6.4±1.3 ppbv h^{-1}), Wuhan (5.8±1.2 ppbv h^{-1}), and Chengdu (4.2±0.9 ppbv h^{-1}) was at a moderate level ($p = 0.08$ and $p = 0.11$ related to Beijing and Wuhan, respectively). HO_2+NO (51.9 - 65.2%) and RO_2+NO (34.6 - 47.3%) were the dominant pathways of O_3 production, in accordance with previous studies in China (Wang H. et al., 2018; Wang Y. et al., 2018; Lyu et al., 2016b, 2019). The higher contributions of RO_2+NO in Beijing (41.5±8.3%) and Lanzhou (47.3±8.5%) than other cities (34.6 - 39.9%) might be attributable to the higher RO_2 concentrations enhanced by the higher local VOCs. In contrast, the prominent destruction pathway of O_3 was OH+NO_2 (45.0 - 72.4%) in all the five cities. However, the second important destruction pathway of O_3 was different in the cities. It was the O_3 reaction with alkenes in Beijing (16.1%) and Lanzhou (29.5%), but photolysis of O_3 in Chengdu (11.8%), Shanghai (18.6%) and Wuhan (19.2%). Overall, the simulated net O_3 production rates among the five cities were consistent with those in previous studies conducted in warm seasons in China. For example, Han et al. (2020) found that the average daytime net O_3 production rate was 11 ppbv h^{-1} during an O_3 episode event in the NCP region in August 2018. Zeng et al. (2019) investigated the net O_3 production rates at three sites in Wuhan during

the summer of 2016 and indicated that the average daily peak net O_3 production rate was 4 ppbv h^{-1} at a roadside site and 10 ppbv h^{-1} at an urban site. Recently, Zhu J.X. et al. (2020) revealed that the net O_3 production rate in an urban area increased from 2.1 ppbv h^{-1} on non-O_3 episode days to 5.6 ppbv h^{-1} on high-O_3 episodes in August 2018 in Wuhan.

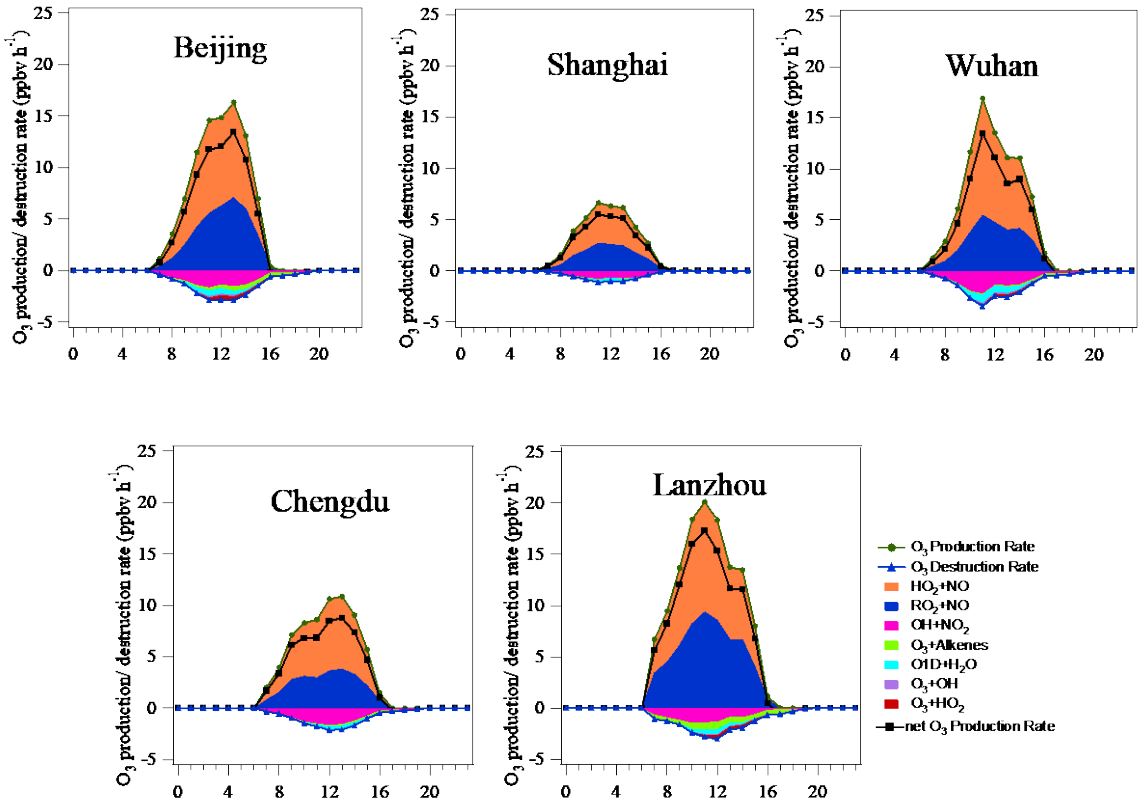

Figure 3. Diurnal variations of the simulated production and destruction rates of O_3 in the five cities.

3.2.3 Cycling of OH radical

Hydroxyl radical (OH) initiates the oxidation of VOCs, promoting atmospheric O_3 formation. Figure 4 illustrates each formation and loss pathway of OH radical in the five cities. Generally, there was a balance between formation and loss rates of OH in all cities. The simulated OH concentration was (3.3±0.7) × 10^6 molecules cm^{-3} in Wuhan, (2.4±0.4) × 10^6 molecules cm^{-3} in Beijing, (2.3±0.6) × 10^6 molecules cm^{-3} in Shanghai, (2.0±0.3) × 10^6 molecules cm^{-3} in Lanzhou, and (1.5±0.3) × 10^6 molecules cm^{-3} in Chengdu (Table S7). The levels of the simulated OH radicals in the five cities were in line with previous studies in urban areas of China. For example, the measured peak OH concentration was (1-8) × 10^6 molecules cm^{-3} in Beijing (Ma. et al.,

2019; Slater et al., 2020), and the daytime average OH concentration was 3.1 × 10^6 molecules cm^{-3} in urban Lanzhou (Wang et al., 2020). In addition, the simulated maximum OH concentration was (3.2 - 6.4) × 10^6 molecules cm^{-3} in Wuhan (Zhu J.X. et al., 2020) and (4 – 8) × 10^6 molecules cm^{-3} in Chengdu (Tan et al., 2018b). Among the formation pathways of OH in all the five cities, HO_2+NO was dominant (83.0 - 85.9%), followed by photolysis of HONO, photolysis of O_3, O_3+VOCs and photolysis of H_2O_2. In comparison, OH was mainly consumed through OH+VOCs (39.8 - 64.5%), followed by OH+CO (13.1 - 35.7%) and OH+NO_2 (11.3 - 18.9%) in the five cities.

RO_x radicals (= hydroxyl radical (OH) + hydroperoxyl radical (HO_2) + organic peroxyl radical (RO_2)) play key roles in O_3 photochemistry, and their concentrations in the atmosphere reflect the atmospheric oxidative capacity (AOC). Table S7 displays the concentration of RO_x in the five cities during the sampling period. It was found that RO_x had comparable concentrations (p>0.1) in Lanzhou ((5.9±1.1) ×10^8 molecules cm^{-3}), Beijing ((5.3±1.1) ×10^8 molecules cm^{-3}) and Wuhan ((4.3±1.0) ×10^8 molecules cm^{-3}), while it was much lower (p < 0.05) in Shanghai ((2.7±0.9) ×10^8 molecules cm^{-3}) and Chengdu ((2.0±0.5) ×10^8 molecules cm^{-3}), indicating that the AOC was stronger and O_3 pollution was more serious in northern and central China in summer.

386

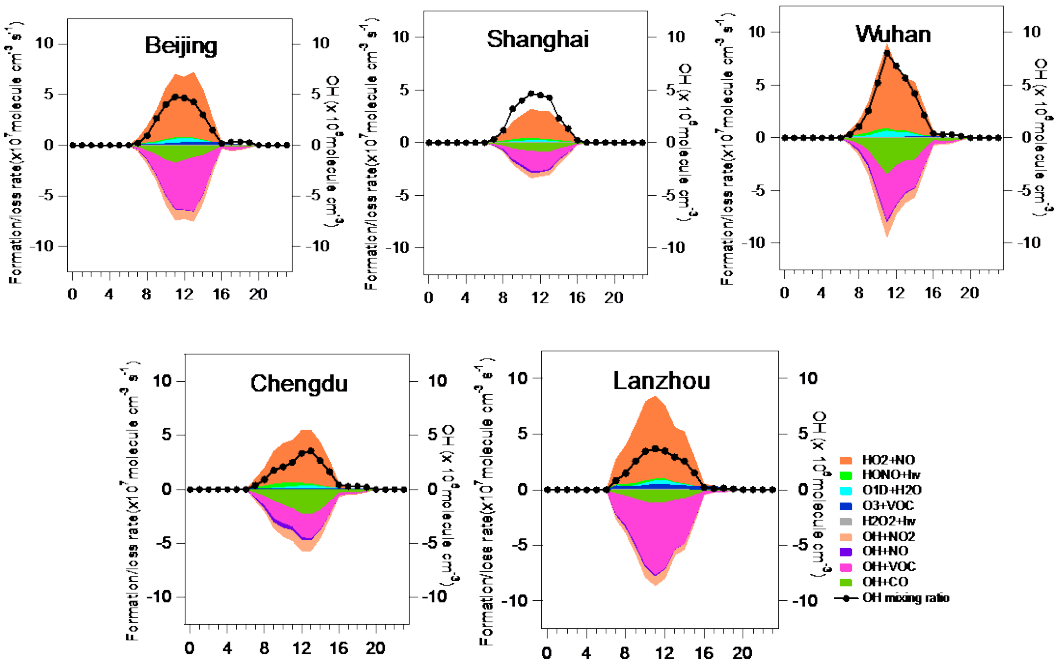

387

388 Figure 4. Average diurnal profiles of the simulated OH formation and loss rates in the five
389 cities.
390

391 **3.3 VOC source identification and source contributions to O_3 formation**

392 **3.3.1 Source apportionment**

393 In the five cities, NO_x and 21 VOC species including 10 alkanes, 5 alkenes/alkynes and 6
394 aromatics in 199 out of the 207 VOC samples were processed by PMF model for source
395 identification and quantification. Note: 8 samples were not used as there were no corresponding
396 NO_x values for these samples. The selection of the 22 species was based on the criteria: 1) their
397 abundances and 2) tracers of NO_x and VOC sources. To reduce the uncertainty of the source
398 apportionment results, compared to separate source apportionments for each city, the samples
399 collected in all the five cities as a whole were used for model input (Text S1). Figure 5 shows
400 the six sources resolved based on the distributions of the NO_x and VOC tracers. The first source,
401 having moderate to high levels of propane and *i*-/*n*-butanes, represented LPG usage (Jorquera,
402 et al., 2004; Guo et al., 2013; Wu F. et al., 2016; Wu R. et al., 2016; Lyu et al., 2017b, 2019;
403 Song et al., 2017). The considerable loadings of *i*-*n*-pentanes and *n*-hexane and moderate
404 amount of C_2 hydrocarbons suggested the second source as gasoline exhaust (Liu et al., 2008a;
405 Ho et al., 2009; Ling and Guo, 2014; Lyu et al., 2019). The third source containing moderate

levels of C_6-C_9 hydrocarbons, benzene and high percentages of NO_x and C_2-C_3 hydrocarbons especially alkenes, which was defined as diesel exhaust (Liu et al., 2008a, c; Sahoo et al., 2011; Lyu et al., 2019). Considering the great amount of 1,3-butadiene and styrene, and moderate loadings of NO_x and aromatics, the fourth source was assigned to industrial emissions (Liu et al., 2008a, c; Knighton et al., 2012; Jones, 2014). The fifth source was more related to solvent usage due to the high levels of C_7-C_9 aromatics (Yuan et al., 2010; Ling and Guo, 2014; Shao et al., 2016). Lastly, the source of biogenic emission was identified because of the dominance of isoprene in factor 6 (Guenther, 2006).

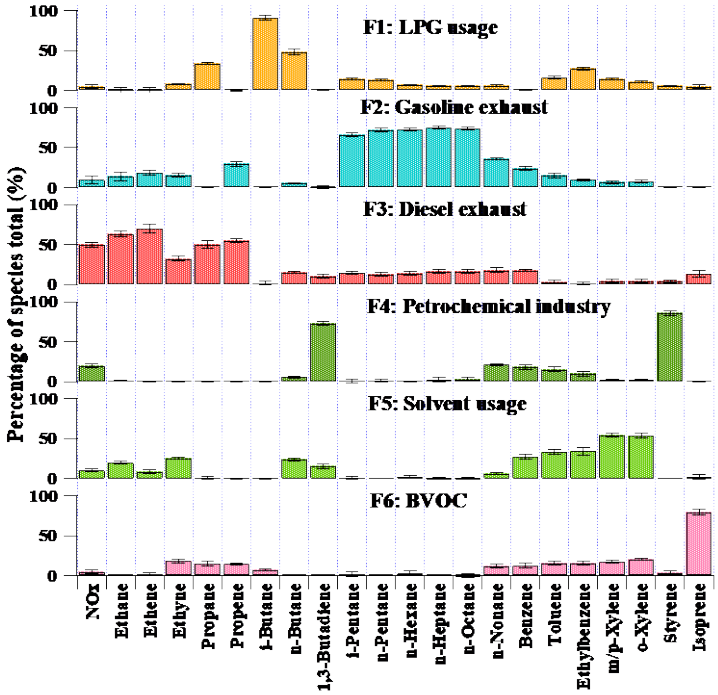

Figure 5. Average profile of the six sources in the five cities extracted from PMF.

3.3.2 Source contribution to VOCs and O_3 production

Table 1 presents the contribution of each source to ambient VOC mixing ratios and to O_3 production in the five cities. Note that the uncertainty of each value was at a considerable level (*i.e.,* at an average of 31.0% of their mean values), which might be due to the limited number of VOC samples collected in each city. Among the six sources, vehicular exhausts, including gasoline exhaust and diesel exhaust, contributed the most to VOC mixing ratios in all the five

423 cities (39.1-53.9%). Diesel exhaust ranked first (26.5-34.0%) in the other four cities except
424 Lanzhou, where both gasoline exhaust (23.9±7.0%) and industrial emissions (23.1±7.8%)
425 contributed the most to VOCs. Elevated contribution of vehicle exhausts to ambient VOCs (27-
426 62%) has been widely reported in NCP (Yuan et al., 2009; Han et al., 2015; Wang et al., 2016;
427 Song et al., 2019), YRD (Wang et al., 2013; An et al., 2017; Liu Y. et al., 2019) and Sichuan
428 Basin (SCB) regions (Zhang et al., 2014; Li et al., 2018). Apart from traffic related sources,
429 solvent usage was the second VOC source in Shanghai, Chengdu and Beijing (15.4-22.5%),
430 and LPG usage had a considerable contribution in Wuhan (19.6±8.0%), which were all
431 consistent with the previous studies, in which solvent usage contributed 19-32% in Shanghai
432 (Cai et al., 2010; Wang et al., 2013; Liu Y. et al., 2019) and 13-23.7% in SCB region (Zhang
433 et al., 2014; Li et al., 2018), and LPG usage accounted for 19.8% in Wuhan (Lyu et al., 2016).
434 In comparison, Lanzhou had the largest industrial emissions (23.1±7.8%) among the five cities,
435 consistent with the contribution of 23.2% reported by Jia et al. (2016). Compared to
436 anthropogenic sources, the contribution of biogenic emissions (4.6-7.2%) was the smallest,
437 consistent with the findings of previous studies (*e.g.*, Wang et al., 2013; Li et al., 2016; Song
438 et al., 2018; Zeng et al., 2018).
439 Regarding the contribution of the six sources to O_3 production in each city, the biogenic
440 emission in the cities except Chengdu was more obvious than other sources, likely due to the
441 high loadings of NO_x, which led to negative contributions of vehicular exhausts and industrial
442 sources to O_3 production in the cities except Lanzhou, where the O_3 production seemed to be
443 controlled by NO_x. In addition, lower photochemical reactivity of VOC species in LPG usage
444 and solvent usage than that in biogenic emission was the reason of less contribution to O_3
445 production. Furthermore, among the anthropogenic sources, gasoline exhaust in Beijing, LPG
446 usage in Wuhan, solvent usage in Chengdu, and both LPG usage and industrial emissions in
447 Lanzhou were the top contributors to local O_3 production.

448 Table 1. Source contributions to VOC mixing ratios and O_3 production in the five cities.

Sources	LPG usage	Gasoline exhaust	Diesel exhaust	Industrial emissions	Solvent usage	BVOC
Contribution to VOCs mixing ratio (%)						

Beijing	13.5±5.2	19.9±5.0	34.0±11.0	10.0±4.0	15.4±5.1	7.2±1.1
Shanghai	13.4±2.6	18.1±4.0	27.0±5.6	12.7±2.9	22.5±3.5	6.4±0.7
Wuhan	19.6±8.0	21.0±8.3	24.6±12.1	15.2±5.7	12.9±3.6	6.6±0.8
Chengdu	17.2±3.8	12.6±6.4	26.5±7.4	18.2±10.9	20.9±4.9	4.6±2.0
Lanzhou	15.7±8.5	23.9±7.0	19.1±3.9	23.1±7.8	11.9±5.5	6.4±1.0
Contribution to O_3 production (%)						
Beijing	0.1±0.2	3.2±0.5	-5.2±2.7	-2.8±0.9	0.5±0.4	5.4±0.6
Shanghai	0.2±0.4	0.7±0.7	-11.2±3.2	-6.2±1.9	0.3±0.8	2.4±0.6
Wuhan	3.6±0.5	-0.1±0.3	-11.6±2.6	-4.5±0.9	0.1±0.3	5.7±0.8
Chengdu	0.6±0.2	-2.6±0.5	-14.9±2.6	-2.5±0.8	7.7±1.3	1.6±0.3
Lanzhou	3.1±0.3	2.3±0.5	2.3±2.8	2.9±1.0	1.9±0.4	5.1±0.5

3.4 Potential control measures for O_3 pollution

3.4.1 O_3-precursor relationship

Figure 6 illustrates the average O_3-integrated RIRs of O_3 precursors during the sampling period in the five cities. The local O_3 formation in Shanghai, Wuhan and Chengdu was limited by VOCs (in particular anthropogenic VOCs (AVOCs)), whereas the negative RIRs of NO_x indicated that cutting NO_x would cause the increase of O_3. In Lanzhou, the local O_3 formation was co-limited by VOCs and NO_x, but more sensitive to the variations of VOCs. In Beijing, the NO_x reduction led to either increase or decrease of O_3 formation on different sampling days given the RIR values ranged from positive to negative values, implying the complexity of local O_3 formation in these five cities. Among different AVOC groups, O_3 formation was more sensitive to OVOCs in Beijing and Wuhan, accounting for 46.7% and 35.6% of the total RIRs of AVOCs, respectively, while aromatics and OVOCs made comparable contributions in Shanghai (aromatics: 28.4%; OVOCs: 29.5%) and Chengdu (aromatics: 33.2%; OVOCs: 30.9%). In Lanzhou, alkenes contributed the most to the total RIR value of AVOCs (43.1%), followed by aromatics (29.6%). In comparison, cities in south part of China, *i.e.,* Chengdu, Shanghai and Wuhan, had relatively larger RIR values of biogenic VOCs (BVOCs), indicating the higher vegetation emissions of BVOCs in summer in the lower mid-latitude areas of China. Furthermore, we investigated the average RIR values during high O_3 period, *i.e.,* when hourly O_3 mixing ratio reached maximum on each sampling day, in the five cities (Figure S2). It was found that O_3 formation in Beijing and Wuhan tended to be co-limited by both VOCs and NO_x,

while it was more sensitive to NO_x in Lanzhou, indicating cutting NO_x might be more effective for O_3 alleviation during high O_3 period in these cities.

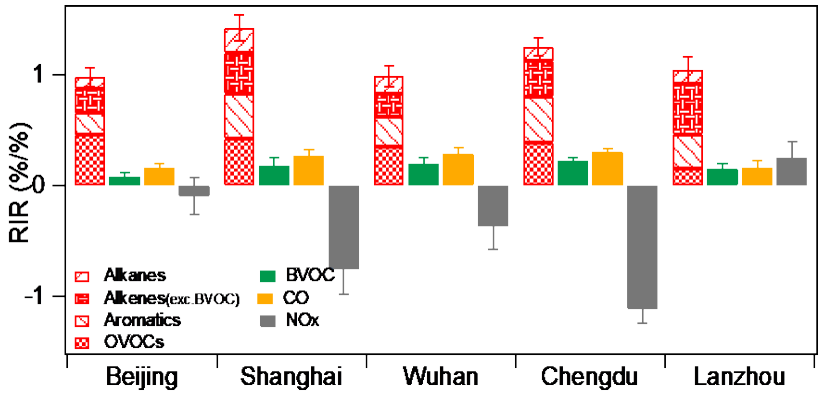

Figure 6. Average O_3-integrated RIRs of precursors, *i.e.*, AVOCs, BVOCs, CO and NO_x on VOC sampling days in the five cities. AVOCs are further categorized into alkanes, alkenes (excluding BVOCs), aromatics and OVOCs, which refer to the 18 C_2-C_{10} alkanes, 13 C_2-C_7 alkenes and alkynes, 10 C_6-C_9 aromatics and 4 C_1-C_3 OVOCs, respectively. BVOCs include isoprene and α-/β-pinenes. Error bars denote the 95% confidence level (C.I.) of each value hereinafter.

Since O_3 formation was more sensitive to VOCs in all cities, the relative impact of individual VOC species on O_3 formation was further examined. Figure 7 presents the average RIR values of top 13 VOCs in each city, including 12 AVOCs and isoprene. The total RIR values of the 13 VOCs held 75.7 - 96.8% of the overall RIR values in the five cities, highlighting the dominant role of a small number of VOC species in local O_3 formation. It was found that among the AVOC species, formaldehyde, acetaldehyde and xylenes had high RIR values in all the five cities, except for acetaldehyde in Lanzhou. In addition, propene had the third largest RIR values among all VOC species in Beijing and Lanzhou. Moreover, trimethylbenzenes and 1-butene were also the key VOC species contributing to O_3 formation in Shanghai.

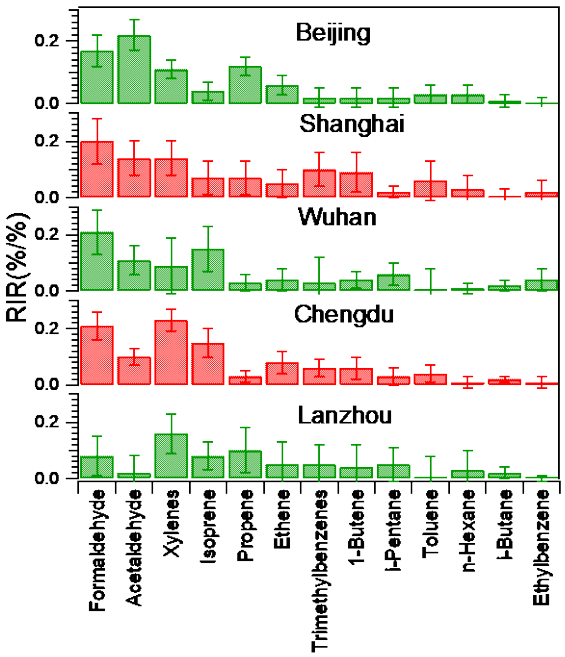

Figure 7. Average RIR values of top 13 VOC species in the five cities.

3.4.2 O_3 control measures

The isopleths of net O_3 production rate in the five cities, based upon the percentages of OH reactivity values with VOCs (OH reactivity$_{VOCs}$) and NO_x (OH reactivity$_{NO_x}$), are plotted in Figure 8. In the five cities, the average OH reactivity$_{VOCs}$ on each sampling day were within the range of 48-193% of the average OH reactivity$_{VOCs}$ of all VOC sampling days. For OH reactivity$_{NO_x}$, the range was 37-173%. Based on a series of hypothetical scenarios with different OH reactivity values of VOCs and NO_x, we simulated the net O_3 production rates in each city using the PBM-MCM model. To include the OH reactivity$_{VOCs}$ and OH reactivity$_{NO_x}$ values on all sampling days, factors between 0 and 200% with the interval of 10% were implemented to the average diurnal profiles of both VOCs and NO_x in each city. In each scenario, the concentrations of VOCs and NO_x were constrained to these scaled factors. Other air pollutants and meteorological conditions were consistent with the base case, which had 100% input of both VOCs and NO_x. It was found that the simulated net O_3 production rate reached the maximum at noon (12:00 LT). Therefore, Figure 8 presents the isopleth of net O_3 production rate at noon in the five cities.

Text S2 introduces the method to define the O_3 formation regimes in each city. According to the simulations, O_3 formation (*i.e.,* base case shown in Figure 8) during the sampling period

was mainly VOCs-limited in Chengdu and Shanghai, co-limited by both VOCs and NO_x in Beijing and Wuhan, but NO_x-limited in Lanzhou. It is consistent with the results on high O_3 hours in section 3.4.1. In Chengdu and Shanghai, the results suggested controlling VOCs be effective to mitigate O_3 formation, whereas reducing NO_x too fast would result in more local O_3 production. However, cutting either VOCs or NO_x would effectively lower O_3 production in Beijing and Wuhan, while reducing NO_x would be more effective than cutting VOCs in Lanzhou. Further, it was found that the local O_3 formation on O_3 episode days (*i.e.,* blue blocks in Figure 8) were in either transitional or NO_x-limited regime in Beijing, Wuhan, and Lanzhou, and in VOC-limited regime in Chengdu, basically in line with the average profile in each city. However, the net O_3 production rates on non-O_3 episode days were not consistent in each city, which deserves more attention when making local control policies.

(a) Limited by VOCs:

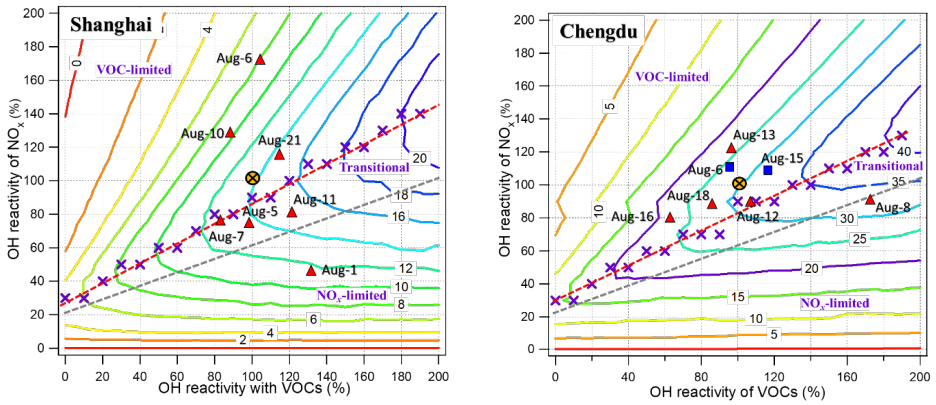

(b) Co-limited by both VOCs and NO_x:

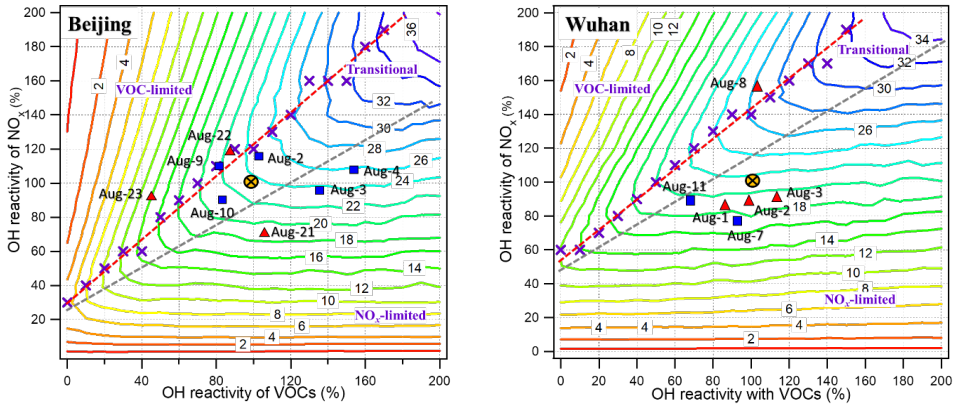

(c) Limited by NO_x:

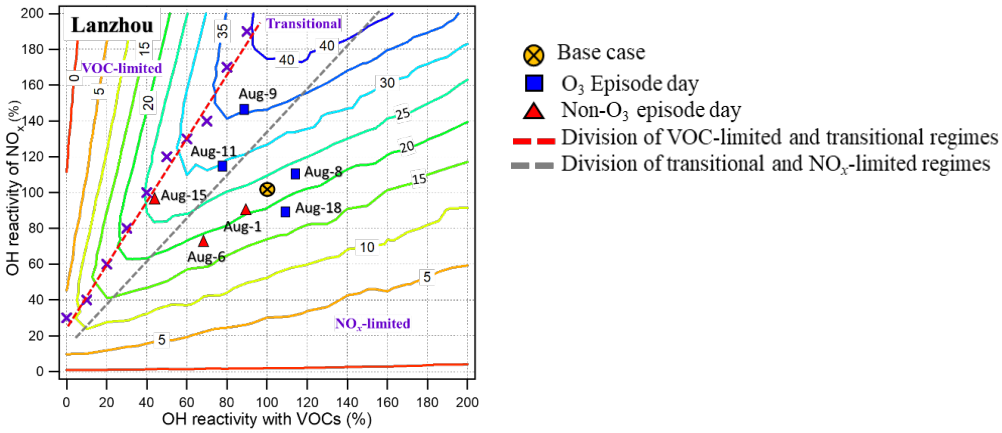

Figure 8. Average isopleths of the net O_3 production rate (ppbv h^{-1}) at noon (12:00 LT) based on the variations of OH reactivity of VOCs* and NO_x** on all VOC sampling days in the five cities. The purple cross represents the OH reactivity of VOCs and NO_x at noon with the maximum net O_3 production rate at a certain OH reactivity$_{VOCs}$. The black cross with circle in yellow refers to the base case with 100% of both OH reactivity$_{VOCs}$ and OH reactivity$_{NOx}$ at noon. The blue blocks and red triangles stand for the OH reactivity of VOCs and NO_x values at noon on O_3 episode days and non-O_3 episode days, respectively.

*OH reactivity of VOCs=$\sum(k_i * [VOC]_i)$, where k_i represents the constant reaction rate of OH with individual VOC species, $[VOC]_i$ means the concentration of individual VOC species.

**OH reactivity of NO_x=$\sum(k_{(OH+NO)} * [NO] + k_{(OH+NO2)} * [NO_2])$, where $k_{(OH+NO)}$ and $k_{(OH+NO2)}$ are the rate constants of OH with NO and NO_2, respectively; [NO] and $[NO_2]$ represent the concentrations of NO and NO_2, respectively.

4. Conclusions

An intensive sampling campaign was concurrently carried out in five Chinese megacities in summer 2018. O_3 pollution in northern and central China, *i.e.,* Beijing, Lanzhou, and Wuhan, was found to be more severe. Further, higher VOC concentrations were found in northern China, *i.e.*, Beijing and Lanzhou. Among these five cities, alkanes and/or OVOCs were the main contributors of TVOCs.

Aromatics and OVOCs were the largest contributors and made comparable contributions to O_3 formation in Chengdu and Shanghai, dominated by xylenes, formaldehyde, and acetaldehyde, while OVOCs contributed the most in Beijing and Wuhan. Alkenes, *i.e.*, isoprene and propene, caused more O_3 formation in Lanzhou. The simulated net O_3 production rate in Lanzhou was the largest, followed by Beijing, Wuhan and Chengdu, while it was the lowest in Shanghai. In

addition, the simulated RO_x concentrations were comparable in Lanzhou, Beijing and Wuhan, which were significantly higher than those in Shanghai and Chengdu, implying stronger atmospheric oxidative capacity and more severe O_3 pollution in northern and central China in summer.

Six sources of O_3 precursors were identified in the five cities, among which vehicular emissions contributed the most to ambient VOCs. Gasoline exhaust in Beijing, LPG usage in Wuhan, solvent usage in Chengdu, and both LPG usage and industrial emissions in Lanzhou were the major sources for local O_3 mitigation.

O_3 formation in Shanghai and Chengdu was typically limited by VOCs. However, it was limited by VOCs during low O_3 period, but co-limited by both VOCs and NO_x during high O_3 period in Beijing and Wuhan. In Lanzhou, O_3 formation was mainly controlled by NO_x when O_3 was intensively produced. Specifically, reducing either VOCs or NO_x would effectively mitigate O_3 formation in Beijing and Wuhan, while cutting NO_x would be more effective than cutting VOCs in Lanzhou. The findings are valuable for the cities to formulate and implement appropriate control measures on O_3 precursors.

Acknowledgements

This study was supported by the Research Grants Council of the Hong Kong Special Administrative Region via Theme-Based Research Scheme (T24-504/17-N) and General Research Fund (PolyU15212421), the National Key R&D Program of China via grant No. 2017YFC0212001, and the Strategic Focus Area scheme of The Research Institute for Sustainable Urban Development at The Hong Kong Polytechnic University (1-BBW9).

References

An, J., Wang, J., Zhang, Y. and Zhu, B., 2017. Source apportionment of volatile organic compounds in an urban environment at the Yangtze River Delta, China. Archives of Environmental Contamination and Toxicology, 72(3), 335-348.

Ashmore, M.R., 2005. Assessing the future global impacts of ozone on vegetation. Plant Cell and Environment, 28 (8), 949–964.

Bell, M.L., McDermott, A., Zeger, S.L., Samet, J.M. and Dominici, F., 2004. Ozone and short-term mortality in 95 US urban communities, 1987-2000. Journal of the American Medical Association, 292(19), 2372-2378.

579 Brown, S. G., Frankel, A., and Hafner, H. R., 2007. Source apportionment of VOCs in the Los
580 Angeles area using positive matrix factorization, Atmospheric Environment, 41, 227-237.

581 Cai, C., Geng, F., Tie, X., Yu, Q. and An, J., 2010. Characteristics and source apportionment
582 of VOCs measured in Shanghai, China. Atmospheric Environment, 44(38), 5005-5014.

583 Cardelino, C.A. and Chameides, W.L., 1995. An observation-based model for analyzing ozone
584 precursor relationships in the urban atmosphere. Journal of the Air and Waste Management
585 Association, 45(3), 161-180.

586 Carter, W.P., 1994. Development of ozone reactivity scales for volatile organic compounds.
587 Air Waste, 44 (7), 881-899.

588 China Council for International Cooperation on Environment and Development (CCICED),
589 2019. Targets and Paths for environmental quality improvement by 2035.
590 http://www.cciced.net/zcyj/yjbg/zcyjbg/2019/201908/P020190830109949890545.pdf (last
591 access: 28 April 2021).

592 Chinese Meteorological Administration (CMA), 2019. China Climate Bulletin of 2018.
593 http://zwgk.cma.gov.cn/zfxxgk/gknr/qxbg/201903/t20190319_1709281.html (last access: 28
594 April 2021).

595 Duan, J., Tan, J., Yang, L., Wu, S. and Hao, J., 2008. Concentration, sources and ozone
596 formation potential of volatile organic compounds (VOCs) during ozone episode in Beijing.
597 Atmospheric Research, 88(1), 25-35.

598 Geng, F.H., Zhang, Q., Tie, X.X., Huang, M.Y., Ma, X.C., Deng, Z.Z., Yu, Q., Quan, J.N.,
599 Zhao, C.S., 2009. Aircraft measurements of O_3, NO_x, CO, VOCs, and SO_2 in the Yangtze River
600 Delta region. Atmospheric Environment, 43, 584–593.

601 Guenther, A., Karl, T., Harley, P., Wiedinmyer, C., Palmer, P.I. and Geron, C., 2006. Estimates
602 of global terrestrial isoprene emissions using MEGAN (model of emissions of gases and
603 aerosols from nature). Atmospheric Chemistry and Physics, 6, 11, 3181-3210.

604 Guo, H., Ling, Z. H., Cheung, K., Wang, D. W., Simpson, I. J., and Blake, D. R., 2013. Acetone
605 in the atmosphere of Hong Kong: Abundance, sources and photochemical precursors,
606 Atmospheric Environment, 65, 80-88.

607 Guo, H., Ling, Z.H., Cheng, H.R., Simpson, I.J., Lyu, X.P., Wang, X.M., Shao, M., Lu, H.X.,
608 Ayoko, G., Zhang, Y.L. and Saunders, S.M., 2017. Tropospheric volatile organic compounds
609 in China. Science of the Total Environment, 574, 1021-1043.

610 Han, M., Lu, X., Zhao, C., Ran, L. and Han, S., 2015. Characterization and source
611 apportionment of volatile organic compounds in urban and suburban Tianjin, China. Advances
612 in Atmospheric Sciences, 32(3), 439-444.

613 Han, S., Yao, Q., Tie, X., Zhang, Y., Zhang, M., Li, P. and Cai, Z. 2020. Analysis of surface
614 and vertical measurements of O_3 and its chemical production in the NCP region, China.
615 Atmospheric Environment, 241, 117759.

Ho, K.F., Lee, S.C., Ho, W.K., Blake, D.R., Cheng, Y., Li, Y.S., Ho, S.S.H., Kung, K., Louise, P.K.K. and Park, D., 2009. Vehicular emission of volatile organic compounds (VOCs) from a tunnel study in Hong Kong. Atmospheric Chemistry and Physics, 9 (19), 7491-7504.

Huang, J.P., Fung, J.C., Lau, A.K. and Qin, Y., 2005. Numerical simulation and process analysis of typhoon-related ozone episodes in Hong Kong. Journal of Geophysical Research: Atmospheres, 110(D05301).

Hui, L., Liu, X., Tan, Q., Feng, M., An, J., Qu, Y., Zhang, Y. and Jiang, M., 2018. Characteristics, source apportionment and contribution of VOCs to ozone formation in Wuhan, Central China. Atmospheric Environment, 192, 55-71.

Jenkin, M. E., Saunders, S. M., and Pilling, M. J., 1997 The tropospheric degradation of volatile organic compounds: a protocol for mechanism development. Atmospheric Environment, 31, 81-104.

Jenkin, M. E., Saunders, S. M., Wagner, V., and Pilling, M. J., 2003. Protocol for the development of the Master Chemical Mechanism, MCM v3 (Part B): tropospheric degradation of aromatic volatile organic compounds. Atmospheric Chemistry and Physics, 3, 181-193.

Jia, C., Mao, X., Huang, T., Liang, X., Wang, Y., Shen, Y., Jiang, W., Wang, H., Bai, Z., Ma, M., Yu, Z., Ma, J. and Gao, H., 2016. Non-methane hydrocarbons (NMHCs) and their contribution to ozone formation potential in a petrochemical industrialized city, Northwest China. Atmospheric Research, 169, 225-236.

Jones, M.D., 2014. Catalytic transformation of ethanol into 1, 3-butadiene. Chemistry Central Journal, 8(1), 1-5.

Jorquera, H. and Rappenglück, B., 2004. Receptor modeling of ambient VOC at Santiago, Chile. Atmospheric Environment, 38(25), 4243-4263.

Knighton, W.B., Herndon, S.C., Wood, E.C., Fortner, E.C., Onasch, T.B., Wormhoudt, J., Kolb, C.E., Lee, B.H., Zavala, M., Molina, L. and Jones, M., 2012. Detecting fugitive emissions of 1, 3-butadiene and styrene from a petrochemical facility: An application of a mobile laboratory and a modified proton transfer reaction mass spectrometer. Industrial and Engineering Chemistry Research, 51(39), 12706-12711.

Lam, S.H.M., Saunders, S.M., Guo, H., Ling, Z.H., Jiang, F., Wang, X.M. and Wang, T.J., 2013. Modelling VOC source impacts on high ozone episode days observed at a mountain summit in Hong Kong under the influence of mountain-valley breezes. Atmospheric Environment, 81, 166-176.

Lee, E., Chan, C. K., and Paatero, P., 1999. Application of positive matrix factorization in source apportionment of particulate pollutants in Hong Kong. Atmospheric Environment, 33, 3201-3212.

Li, J., Wu, R., Li, Y., Hao, Y., Xie, S. and Zeng, L., 2016. Effects of rigorous emission controls on reducing ambient volatile organic compounds in Beijing, China. Science of the Total Environment, 557, 531-541.

Li, J., Zhai, C., Yu, J., Liu, R., Li, Y., Zeng, L. and Xie, S., 2018. Spatiotemporal variations of ambient volatile organic compounds and their sources in Chongqing, a mountainous megacity in China. Science of the Total Environment, 627, 1442-1452.

Li, K., Jacob, D. J., Liao, H., Shen, L., Zhang, Q. and Bates, K. H., 2019. Anthropogenic drivers of 2013-2017 trends in summer surface ozone in China. Proceedings of the National Academy of Sciences, 116(2), 422-427.

Li, M., Zhang, Q., Zheng, B., Tong, D., Yu, L., Liu, F., Hong, C., Kang, S., Liu, Y., Zhang, Y. and Yu, B., 2019. Persistent growth of anthropogenic non-methane volatile organic compound (NMVOC) emissions in China during 1990–2017: Drivers, speciation and ozone formation potential. Atmospheric Chemistry and Physics, 19(13), 8897-8913.

Ling, Z.H. and Guo, H., 2014. Contribution of VOC sources to photochemical ozone formation and its control policy implication in Hong Kong. Environmental Science and Policy, 38, 180-191.

Ling, Z.H., Guo, H., Lam, S.H.M., Saunders, S.M. and Wang, T., 2014. Atmospheric photochemical reactivity and ozone production at two sites in Hong Kong: Application of a master chemical mechanism–photochemical box model. Journal of Geophysical Research: Atmospheres, 119(17), 10567-10582.

Liu, X., Lyu, X., Wang, Y., Jiang, F. and Guo, H., 2019. Intercomparison of O_3 formation and radical chemistry in the past decade at a suburban site in Hong Kong. Atmospheric Chemistry and Physics, 19(7), 5127-5145.

Liu, X., Wang, N., Lyu, X., Zeren, Y., Jiang, F., Wang, X., Zou, S., Ling, Z. and Guo, H., 2020. Photochemistry of ozone pollution in autumn in Pearl River Estuary, South China. Science of The Total Environment, 754, 141812.

Liu, Y., M. Shao, L. Fu, S. Lu, L. Zeng and D. Tang, 2008a. Source profiles of volatile organic compounds (VOCs) measured in China: Part I. Atmospheric Environment, 42, 6247-6260.

Liu, Y., Shao, M., Chang, C. C., Wang, J. L. and Chen, G. 2008b. Volatile Organic Compound (VOC) measurements in the Pearl River Delta (PRD) region, China. Atmospheric Chemistry and Physics,8, 1531-1545.

Liu, Y., Shao, M., Lu, S., Chang, C.C., Wang, J.L. and Fu, L., 2008c. Source apportionment of ambient volatile organic compounds in the Pearl River Delta, China: Part II. Atmospheric Environment, 42(25), 6261-6274.

Liu, Y.H., Wang, H., Jing, S., Gao, Y., Peng, Y., Lou, S., Cheng, T., Tao, S., Li, L., Li, Y., Huang, D., Wang, Q. and An, J., 2019. Characteristics and sources of volatile organic

compounds (VOCs) in Shanghai during summer: Implications of regional transport. Atmospheric Environment, 215, 116902.

Liu, Y.M. and Wang, T., 2020a. Worsening urban ozone pollution in China from 2013 to 2017–Part 1: The complex and varying roles of meteorology. Atmospheric Chemistry and Physics, 20(11), 6305-6321.

Liu, Y.M. and Wang, T., 2020b. Worsening urban ozone pollution in China from 2013 to 2017–Part 2: The effects of emission changes and implications for multi-pollutant control. Atmospheric Chemistry and Physics, 20(11), 6323-6337.

Liu, Z., Wang, Y., Gu, D., Zhao, C., Huey, L. G., Stickel, R., Liao, J., Shao, M., Zhu, T., Zeng, L., Amoroso, A., Costabile, F., Chang, C. C. and Liu, S. C., 2012. Summertime photochemistry during CAREBeijing-2007: RO_x budgets and O_3 formation. Atmospheric Chemistry and Physics, 12, 7737-7752.

Lu, H., Lyu, X., Cheng, H., Ling, Z. and Guo, H., 2019. Overview on the spatial-temporal characteristics of the ozone formation regime in China. Environmental Science: Process Impacts, 21, 916-929.

Lu, X., Chen, N., Wang, Y., Cao, W., Zhu, B., Yao, T., Fung, J.C. and Lau, A.K., 2017. Radical budget and ozone chemistry during autumn in the atmosphere of an urban site in central China. Journal of Geophysical Research: Atmospheres, 122(6), 3672-3685.

Lu, X., Zhang, L., Chen, Y.F., Zhou, M., Zheng, B., Li, K., Liu, Y.M., Lin, J.T., Fu, T.M. and Zhang, Q., 2019. Exploring 2016-2017 surface ozone pollution over China: source contributions and meteorological influences. Atmospheric Chemistry and Physics, 19, 8339–8361.

Lu, X., Zhang, L., Wang, X., Gao, M., Li, K., Zhang, Y., Yue, X. and Zhang, Y., 2020a. Rapid Increases in Warm-Season Surface Ozone and Resulting Health Impact in China Since 2013. Environmental Science and Technology Letters, 7, 240-247.

Lu, X., Zhang, S., Xing, J., Wang, Y., Chen, W., Ding, D., Wu, Y., Wang, S., Duan, L. and Hao, J., 2020b. Progress of air pollution control in China and its challenges and opportunities in the ecological civilization era. Engineering, 6(12), 1423-1431.

Lyu, X. P., Ling, Z. H., Guo, H., Saunders, S. M., Lam, S. H. M., Wang, N., Wang, Y., Liu, M., and Wang, T., 2015. Re-examination of C1-C5 alkyl nitrates in Hong Kong using an observation-based model. Atmospheric Environment, 120, 28-37.

Lyu, X.P., Liu, M., Guo, H., Ling, Z.H., Wang, Y., Louie, P.K.K. and Luk, C.W.Y., 2016a. Spatiotemporal variation of ozone precursors and ozone formation in Hong Kong: Grid field measurement and modelling study. Science of The Total Environment, 569, 1341-1349.

Lyu, X. P., Chen, N., Guo, H., Zhang, W. H., Wang, N., Wang, Y. and Liu, M., 2016b. Ambient volatile organic compounds and their effect on ozone production in Wuhan, central China. Science of the Total Environment, 541, 200-209.

Lyu, X.P., Guo, H., Wang, N., Simpson, I.J., Cheng, H., Zeng, L., Saunders, S.M., Lam, S.H.M., Meinardi, S. and Blake, D.R., 2017a. Modeling C1–C4 alkyl nitrate photochemistry and their impacts on O_3 production in urban and suburban environments of Hong Kong. Journal of Geophysical Research: Atmospheres, 122(19), 10539-10556.

Lyu, X.P., Zeng, L.W., Guo, H., Simpson, I.J., Ling, Z.H., Wang, Y., Murray, F., Louie, P.K.K., Saunders, S.M., Lam, S.H.M. and Blake, D.R., 2017b. Evaluation of the effectiveness of air pollution control measures in Hong Kong. Environmental pollution, 220, 87-94.

Lyu, X.P., Wang, N., Guo, H., Xue, L.K., Jiang, F., Zeren, Y.Z., Cheng, H.R., Cai, Z., Han, L.H. and Zhou, Y., 2019. Causes of a continuous summertime O_3 pollution event in Jinan, a central city in the North China Plain. Atmospheric Chemistry and Physics. 19, 5, 3025-3042.

Ma, X., Tan, Z., Lu, K., Yang, X., Liu, Y., Li, S., Li, X., Chen, S., Novelli, A., Cho, C. and Zeng, L., 2019. Winter photochemistry in Beijing: Observation and model simulation of OH and HO2 radicals at an urban site. Science of the Total Environment, 685, 85-95.

Madronich, S. and Flocke, S., 1999. The role of solar radiation in atmospheric chemistry. Environmental Photochemistry, 2, 1-26.

Ministry of Ecology and Environment of the People's Republic of China (MEE PRC), 2018. The State Council issued a notice on the issuance of a three-year Action Plan for Winning the Battle against Blue Skies. http://www.gov.cn/zhengce/content/2018-07/03/content_5303158.htm (last access: 28 April 2021).

Ministry of Ecology and Environment of the People's Republic of China (MEE PRC), 2019. MEE releases Report on Air Quality Improvement in China (2013-2018) https://www.mee.gov.cn/xxgk2018/xxgk/xxgk15/201906/t20190606_705778.html (last access: 28 April 2021).

National Research Council (NRC), 1992. Rethinking the ozone problem in urban and regional air pollution. Washington, DC: National Academies Press. https://doi.org/10.17226/1889.

Ning G., Yim S.H.L., Yang Y., Gu Y. and Dong G., 2020. Modulations of synoptic and climatic changes on ozone pollution and its health risks in mountain-basin areas. Atmospheric Environment, 240, 117808.

Norris, G., Wade, K., and Foley, C., 2008. EPA Positive Matrix Factorization (PMF) 3.0 Fundamentals and User Guide, US Environmental Protection Agency, Office of Research and Development, Washington, EPA 600/R-08/108.

Paatero, P., 1997. Least squares formulation of robust non-negative factor analysis. Chemometrics and Intelligent Laboratory Systems, 37(1), 23-35.

Paatero, P., 2000a. User's Guide for Positive Matrix Factorization Programs PMF2 and PMF3, Part 1: Tutorial, Prepared by University of Helsinki, Finland. US Environmental Protection Agency.

760 Paatero, P., 2000b. User's Guide for Positive Matrix Factorization Programs PMF2 and PMF3,
761 Part 2: Reference, Prepared by University of Helsinki, Finland. US Environmental Protection
762 Agency.

763 Polissar, A. V., Hopke, P. K., Paatero, P., Malm, W. C., and Sisler, J. F., 1998. Atmospheric
764 aerosol over Alaska: 2. Elemental composition and sources, Journal of Geophysical Research:
765 Atmospheres, 103 (D15).

766 Ran, L., Zhao, C., Geng, F., Tie, X., Tang, X., Peng, L., Zhou, G., Yu, Q., Xu, J. and Guenther,
767 A., 2009. Ozone photochemical production in urban Shanghai, China: Analysis based on
768 ground level observations. Journal of Geophysical Research: Atmospheres, 114(D15).

769 Ran, L., Zhao, C. S., Xu, W. Y., Han, M., Lu, X. Q., Han, S. Q., Lin, W. L., Xu, X. B., Gao,
770 W., Yu, Q., Geng, F. H., Ma, N., Deng, Z. Z. And Chen, J., 2012. Ozone production in summer
771 in the megacities of Tianjin and Shanghai, China: a comparative study. Atmospheric Chemistry
772 and Physics, 12, 7531-7542.

773 Reff, A., Eberly, S. I., and Bhave, P. V., 2007. Receptor modeling of ambient particulate matter
774 data using positive matrix factorization: review of existing methods. Journal of the Air and
775 Waste Management Association, 57, 146-154.

776 Sahoo, D., Petersen, B. and Miles, P., 2011. Measurement of equivalence ratio in a light-duty
777 low temperature combustion diesel engine by planar laser induced fluorescence of a fuel tracer.
778 SAE International Journal of Engines, 4(2), 2312-2325.

779 Saunders, S.M., Jenkin, M.E., Derwent, R.G. and Pilling, M.J., 2003. Protocol for the
780 development of the Master Chemical Mechanism, MCM v3 (Part A): Tropospheric degradation
781 of non-aromatic volatile organic compounds. Atmospheric Chemistry and Physics, 3, 161-180.

782 Shao, P., An, J., Xin, J., Wu, F., Wang, J., Ji, D. and Wang, Y., 2016. Source apportionment of
783 VOCs and the contribution to photochemical ozone formation during summer in the typical
784 industrial area in the Yangtze River Delta, China. Atmospheric Research, 176, 64-74.

785 Slater, E.J., Whalley, L.K., Woodward-Massey, R., Ye, C., Lee, J.D., Squires, F., Hopkins,
786 J.R., Dunmore, R.E., Shaw, M., Hamilton, J.F. and Lewis, A.C., 2020. Elevated levels of OH
787 observed in haze events during wintertime in central Beijing. Atmospheric Chemistry and
788 Physics, 20, 14847–14871.

789 Song, C., Liu, B., Dai, Q., Li, H. and Mao, H., 2019. Temperature dependence and source
790 apportionment of volatile organic compounds (VOCs) at an urban site on the north China plain.
791 Atmospheric Environment, 207, 167-181.

792 Song, M., Tan, Q., Feng, M., Qu, Y., Liu, X., An, J. and Zhang, Y., 2018. Source
793 Apportionment and Secondary Transformation of Atmospheric Nonmethane Hydrocarbons in
794 Chengdu, Southwest China. Journal of Geophysical Research: Atmospheres, 123, 9741-9763.

Su, R., Lu, K., Yu, J., Tan, Z., Jiang, M., Li, J., Xie, S., Wu, Y., Zeng, L., Zhai, C. and Zhang, Y., 2017. Exploration of the formation mechanism and source attribution of ambient ozone in Chongqing with an observation-based model. Science China Earth Sciences, 61, 23-32.

Tan, Z., Fuchs, H., Lu, K., Hofzumahaus, A., Bohn, B., Broch, S., Dong, H., Gomm, S., Häseler, R., He, L., Holland, F., Li, X., Liu, Y., Lu, S., Rohrer, F., Shao, M., Wang, B., Wang, M., Wu, Y., Zeng, L., Zhang, Y., Wahner, A. and Zhang, Y., 2017. Radical chemistry at a rural site (Wangdu) in the North China Plain: observation and model calculations of OH, HO2 and RO2 radicals. Atmospheric Chemistry and Physics, 17, 663-690.

Tan, Z., Lu, K., Dong, H., Hu, M., Li, X., Liu, Y., Lu, S., Shao, M., Su, R., Wang, H. and Wu, Y., 2018a. Explicit diagnosis of the local ozone production rate and the ozone-NO_x-VOC sensitivities. Science Bulletin, 63(16), 1067-1076.

Tan, Z., Lu, K., Jiang, M., Su, R., Dong, H., Zeng, L., Xie, S., Tan, Q. and Zhang, Y., 2018b. Exploring ozone pollution in Chengdu, southwestern China: A case study from radical chemistry to O_3-VOC-NO_x sensitivity. Science of the Total Environment, 636, 775-786.

Tang, W., Zhao, C., Geng, F., Peng, L., Zhou, G., Gao, W., Xu, J. and Tie, X., 2008. Study of ozone "weekend effect" in Shanghai. Science in China Series D: Earth Sciences, 51(9), 1354-1360.

Thompson, D.W., Solomon, S., Kushner, P.J., England, M.H., Grise, K.M. and Karoly, D.J., 2011. Signatures of the Antarctic ozone hole in Southern Hemisphere surface climate change. Nature Geoscience, 4(11), 741-749.

United States Environmental Protection Agency (US EPA), 2017. Positive Matrix Factorization Model for environmental data analyses, available at https://www.epa.gov/air-research/positive-matrix-factorization-model-environmental-data-analyses (last access: 28 April 2021).

Wang, B., Shao, M., Lu, S. H., Yuan, B., Zhao, Y., Wang, M., Zhang, S. Q. and Wu, D., 2010. Variation of ambient non-methane hydrocarbons in Beijing city in summer 2008. Atmospheric Chemistry and Physics, 10, 5911-5923.

Wang, G., Cheng, S., Wei, W., Zhou, Y., Yao, S. and Zhang, H., 2016. Characteristics and source apportionment of VOCs in the suburban area of Beijing, China. Atmospheric Pollution Research, 7(4), 711-724.

Wang, G., Jia, S., Li, R., Ma, S., Chen, X., Li, L., Shi, G. and Niu, X., 2020. Seasonal variation characteristics of hydroxyl radical pollution and its potential formation mechanism during the daytime in Lanzhou. Journal of Environmental Sciences, 95, 58-64.

Wang, H., Lyu, X.P., Guo, H., Wang, Y., Zou, S.C., Ling, Z.H., Wang, X.M., Jiang, F., Zeren, Y.Z., Pan, W.Z. and Huang, X.B., 2018. Ozone pollution around a coastal region of South China Sea: interaction between marine and continental air. Atmospheric Chemistry and Physics, 18, 4277-4295.

Wang, H.L., Chen, C.H., Wang, Q., Huang, C., Su, L.Y., Huang, H.Y., Lou, S.R., Zhou, M., Li, L., Qiao, L.P. and Wang, Y.H., 2013. Chemical loss of volatile organic compounds and its impact on the source analysis through a two-year continuous measurement. Atmospheric Environment, 80, 488-498.

Wang, H.X., Kiang, C.S., Tang, X.Y., Zhou, X.J., and Chameides, W.L., 2005. Surface ozone: A likely threat to crops in Yangtze delta of China, Atmospheric Environment, 39, 3843–3850.

Wang M.Y., Yim S.H.L., Wong D.C., Ho K.F., 2019. Source contributions of surface ozone in China using an adjoint sensitivity analysis. Science of the Total Environment, 662, 385-392.

Wang, N., Guo, H., Jiang, F., Ling, Z.H. and Wang, T., 2015. Simulation of ozone formation at different elevations in mountainous area of Hong Kong using WRF-CMAQ model. Science of the Total Environment, 505, 939-951.

Wang, T., Xue, L., Brimblecombe, P., Lam, Y.F., Li, L. and Zhang, L., 2017. Ozone pollution in China: A review of concentrations, meteorological influences, chemical precursors, and effects. Science of the Total Environment, 575, 1582-1596.

Wang, W, Cheng, T., Gu, X., Chen, H., Guo, H., Wang, Y., Bao, F., Shi, S., Xu, B., Zuo, X. and Meng, C., 2017. Assessing spatial and temporal patterns of observed ground-level ozone in China. Scientific Reports, 7(1), 1-12.

Wang, Y., Wang, H., Guo, H., Lyu, X.P., Cheng, H.R., Ling, Z.H., Louie, P.K., Simpson, I.J., Meinardi, S. and Blake, D.R., 2017. Long-term O_3-precursor relationships in Hong Kong: field observation and model simulation. Atmospheric Chemistry and Physics, 17, 10919-10935.

Wang, Y., Guo, H., Zou, S., Lyu, X., Ling, Z., Cheng, H. and Zeren, Y., 2018. Surface O_3 photochemistry over the South China Sea: Application of a near-explicit chemical mechanism box model. Environmental Pollution, 234, 155-166.

Wu, F., Yu, Y., Sun, J., Zhang, J., Wang, J., Tang, G. and Wang, Y., 2016. Characteristics, source apportionment and reactivity of ambient volatile organic compounds at Dinghu Mountain in Guangdong Province, China. Science of the Total Environment, 548, 347-359.

Wu, R., Li, J., Hao, Y., Li, Y., Zeng, L. and Xie, S., 2016. Evolution process and sources of ambient volatile organic compounds during a severe haze event in Beijing, China. Science of the Total Environment, 560, 62-72.

Wu, R. and Xie, S., 2017. Spatial distribution of ozone formation in China derived from emissions of speciated volatile organic compounds. Environmental Science and Technology 51, 2574–2583.

Xu, S.C., Li, Y.W., Miao, Y.M., Gao, C., He, Z.X., Shen, W.X., Long, R.Y., Chen, H., Zhao, B. and Wang, S.X., 2019. Regional differences in nonlinear impacts of economic growth, export and FDI on air pollutants in China based on provincial panel data. Journal of Cleaner Production, 228, 455-466.

Xue, L. K., Wang, T., Gao, J., Ding, A. J., Zhou, X. H., Blake, D. R., Wang, X. F., Saunders, S. M., Fan, S. J., Zuo, H. C., Zhang, Q. Z. and Wang, W. X., 2014a. Ground-level ozone in four Chinese cities: precursors, regional transport and heterogeneous processes. Atmospheric Chemistry and Physics, 14, 13175-13188.

Yang, X., Xue, L., Wang, T., Wang, X., Gao, J., Lee, S., Blake, D. R., Chai, F. and Wang, W., 2018. Observations and Explicit Modelling of Summertime Carbonyl Formation in Beijing: Identification of Key Precursor Species and Their Impact on Atmospheric Oxidation Chemistry. Journal of Geophysical Research: Atmospheres, 123, 1426-1440.

Yuan, B., Shao, M., Lu, S. and Wang, B., 2010. Source profiles of volatile organic compounds associated with solvent use in Beijing, China. Atmospheric Environment, 44(15), 1919-1926.

Yuan, Z., Lau, A.K.H., Shao, M., Louie, P.K., Liu, S.C. and Zhu, T., 2009. Source analysis of volatile organic compounds by positive matrix factorization in urban and rural environments in Beijing. Journal of Geophysical Research: Atmospheres, 114(D2).

Zeng, P., Lyu, X. P., Guo, H., Cheng, H. R., Jiang, F., Pan, W. Z., Wang, Z. W., Liang, S. W. and Hu, Y. Q., 2018. Causes of ozone pollution in summer in Wuhan, Central China. Environmental Pollution, 241, 852-861.

Zeng, P., Lyu, X., Guo, H., Cheng, H., Wang, Z., Liu, X. and Zhang, W., 2019. Spatial variation of sources and photochemistry of formaldehyde in Wuhan, Central China. Atmospheric Environment, 214, 116826.

Zhang, J., Sun, Y., Wu, F., Sun, J. and Wang, Y., 2014. The characteristics, seasonal variation and source apportionment of VOCs at Gongga Mountain, China. Atmospheric Environment, 88, 297-305.

Zhang, Y.L., Wang, X., Blake, D.R., Li, L., Zhang, Z., Wang, S., Guo, H., Lee, S.C., Gao, B., Chan, L., and Wu, D., 2012. Aromatic hydrocarbons as ozone precursors before and after outbreak of the 2008 financial crisis in the Pearl River Delta region, South China. Journal of Geophysical Research: Atmospheres, 117, D15306.

Zhu, J., Wang, S., Wang, H., Jing, S., Lou, S., Saiz-Lopez, A. and Zhou, B., 2020. Observationally constrained modelling of atmospheric oxidation capacity and photochemical reactivity in Shanghai, China. Atmospheric Chemistry and Physics, 20, 1217-1232.

Zhu, J.X., Cheng, H.R., Peng, J., Zeng, P., Wang, Z., Lyu, X.P. and Guo, H., 2020. O_3 photochemistry on O_3 episode days and non-O_3 episode days in Wuhan, Central China. Atmospheric Environment, 223, 117236.

Zhu, Y., Yang, L., Chen, J., Wang, X., Xue, L., Sui, X., Wen, L., Xu, C., Yao, L., Zhang, J. and Shao, M., 2016. Characteristics of ambient volatile organic compounds and the influence of biomass burning at a rural site in Northern China during summer 2013. Atmospheric Environment, 124, 156-165.

Zou, Y., Deng, X.J., Zhu, D., Gong, D.C., Wang, H., Li, F., Tan, H.B., Deng, T., Mai, B.R., Liu, X.T. and Wang, B.G., 2015. Characteristics of 1 year of observational data of VOCs, NO_x and O_3 at a suburban site in Guangzhou, China. Atmospheric Chemistry and Physics, 15(12), 6625-6636.